Materials and Structures (2011) 44:475–486
DOI 10.1617/s11527-010-9642-4

ORIGINAL ARTICLE

Analysis technique for restrained shrinkage of concrete containing chlorides

Sang Soon Park · Seung-Jun Kwon · Ha-Won Song

Received: 2 April 2009 / Accepted: 15 July 2010 / Published online: 30 July 2010

Abstract Cracks in concrete containing chlorides easily occur due to restraint conditions and they can be the main reasons of durability and safety issues. In this paper, analysis technique which can handle mixed chloride and its effect on restrained drying shrinkage is proposed. For the evaluation of stress development and cracking time due to restrained drying shrinkage, free and restrained drying shrinkage test are carried out for concrete specimens containing different sodium chloride (NaCl) content. The results show that mixed chloride content increases restraint stress but does not increase strength. Considering the effect of chloride on shrinkage based on the test results, effective restraint stress development and cracking of concrete specimens containing different level of chloride are evaluated through utilizing previously developed models for behaviors in early-age concrete like hydration and moisture transport. The results from this proposed technique are verified by comparison with test results.

Keywords Concrete · Chloride · Restrained shrinkage · Cracks · Moisture transport

S. S. Park
Civil Engineering, Sangmyung University, Chungnam, Chunan, Anseo dong 300, South Korea
e-mail: parkss87@smu.ac.kr

S.-J. Kwon (✉)
Civil and Environmental Engineering, University of California, Irvine, CA 92617, USA
e-mail: jjuni98@yonsei.ac.kr

H.-W. Song
Civil Engineering, Yonsei University, Seoul 120-749, South Korea
e-mail: song@yonsei.ac.kr

1 Introduction

Early-age concrete undergoes heat generation and moisture transport due to hydration and drying process simultaneously, and the stresses and strains are initially induced to the concrete structures due to the restrained condition. When changes in concrete volume due to drying shrinkage are restrained, tensile stresses may develop, and it can propagate to cracking of concrete [1–3]. Although, the induced micro-cracks may not degrade the structural performance immediately, these can affect durability performance by permitting the intrusions of harmful agents such as chloride ions or carbon dioxide [4–6]. Cracking of early-age concrete depends on the relationship between tensile strength of concrete and restraint stress, which is determined by the characteristics such as hydration heat, shrinkage, degree of restraint, Young's modulus, and creep [7, 8]. If elasticity increases rapidly in early-age concrete, tensile stress also increases rapidly before releasing the stress due to relaxation, which may cause cracking in early-age concrete [9]. Furthermore, the evaluation for cracking with restraint stress needs a complicated technique

which is capable of calculating both material behavior like hydration and moisture transport and mechanical behavior like stress and strength development with boundary conditions at the same time [7].

Recently, a great deal of sea-sand is used for concrete manufacturing due to the insufficient aggregate, which is caused by increasing demand on concrete products [10, 11]. Much research on concrete with chloride ion is mainly performed for deterioration analysis like chloride diffusion or steel corrosion [12–14]. For the quantitative deterioration analysis in chloride-mixed concrete, it is important to evaluate the chloride effects on the behavior of drying shrinkage in early-age concrete. If a reinforced concrete structure is exposed to harsh environment, cracks caused by drying shrinkage which may be accelerated by mixed chloride ions can be the main routes for intrusion of deteriorating ions.

In this paper, an analysis technique for cracking resistance is proposed for initially chloride-mixed concrete. For this study, crack-inducing tests in axially confined condition are carried out for the concrete specimens with different chloride contents. For the chloride effect on drying shrinkage, tests for water evaporation and free drying without restraint are performed. Considering the chloride effect on experimental data on drying shrinkage, an analysis technique for the restrained drying shrinkage in concrete with chloride contents is proposed through utilizing the previously developed models [15–19], so called, multi-component hydration heat model (MCHHM), micro-pore structure formation model (MPSFM), and moisture transport model (MTM). Integrated FE analysis using the proposed models is carried out and the reduced cracking time caused by restrained drying shrinkage is evaluated in the concrete with different chloride contents. In this present paper, the experimental and numerical studies are performed for the analysis of restrained drying shrinkage in chloride-contaminated concrete. The material and mechanical behaviors of early-age concrete containing chlorides are also discussed.

2 Experimental program

2.1 Procedures

In this paper, several tests for drying shrinkage under axially restrained condition are performed for concrete with different chloride contents. Test equipments are made of steel plates based on the standard method of drying shrinkage and crack resistance of concrete referring to JIS [20], as shown in Fig. 1. Test specimens are prepared with different chloride contents of 0.00, 0.07, 0.60, and 1.20% of cement weight. They are cured in the humidity chamber under room condition of 25°C temperature and 60% relative humidity (R.H.) for 2 days and then drying test is performed in the condition of 20°C temperature and 60% R.H. For the curing period, the surface of concrete is covered with saturated cloth. After curing period, bottom plate of the frame is detached from the concrete specimen and longitudinal restraint of shrinkage is induced by the two side surfaces of the frame. The cracking time is observed through visual inspection and the restrained strain is measured through strain gauges on the surface of specimen by every 4 h. For measuring the strain of steel frame, 3 strain gauges are attached on each side surface as shown in Fig. 1a. Additionally, the free drying shrinkage and water loss (evaporated water) in concrete specimens are measured in the same exposure condition. The strains of free drying shrinkage are measured through both strain gauges and one contact gauge, and the weight changes in cubic specimens are measured with a scale of 0.01 g unit. The test equipment including restrained drying shrinkage, free drying shrinkage, and weight change in water loss are shown in Fig. 1a, b, c, respectively.

The mix proportion of concrete for this study is listed in Table 1.

2.2 Test results

2.2.1 *Compressive strength and elastic modulus*

For the evaluation of physical characteristics of the specimens, tests for compressive strength and Young's modulus are performed at the age of 3, 7, and 28 days based on JIS [21, 22]. Cylindrical specimens (15 × 30 cm) are used for the tests. The results of compressive strength and Young's modulus are plotted in Fig. 2a, b with the results of regression analysis.

As shown in Fig. 2, no clear development of strength is measured with respect to the chloride content for 28 days. In the test of Young's modulus, similar trend showing little difference is evaluated. The regression results for strength and elastic modulus

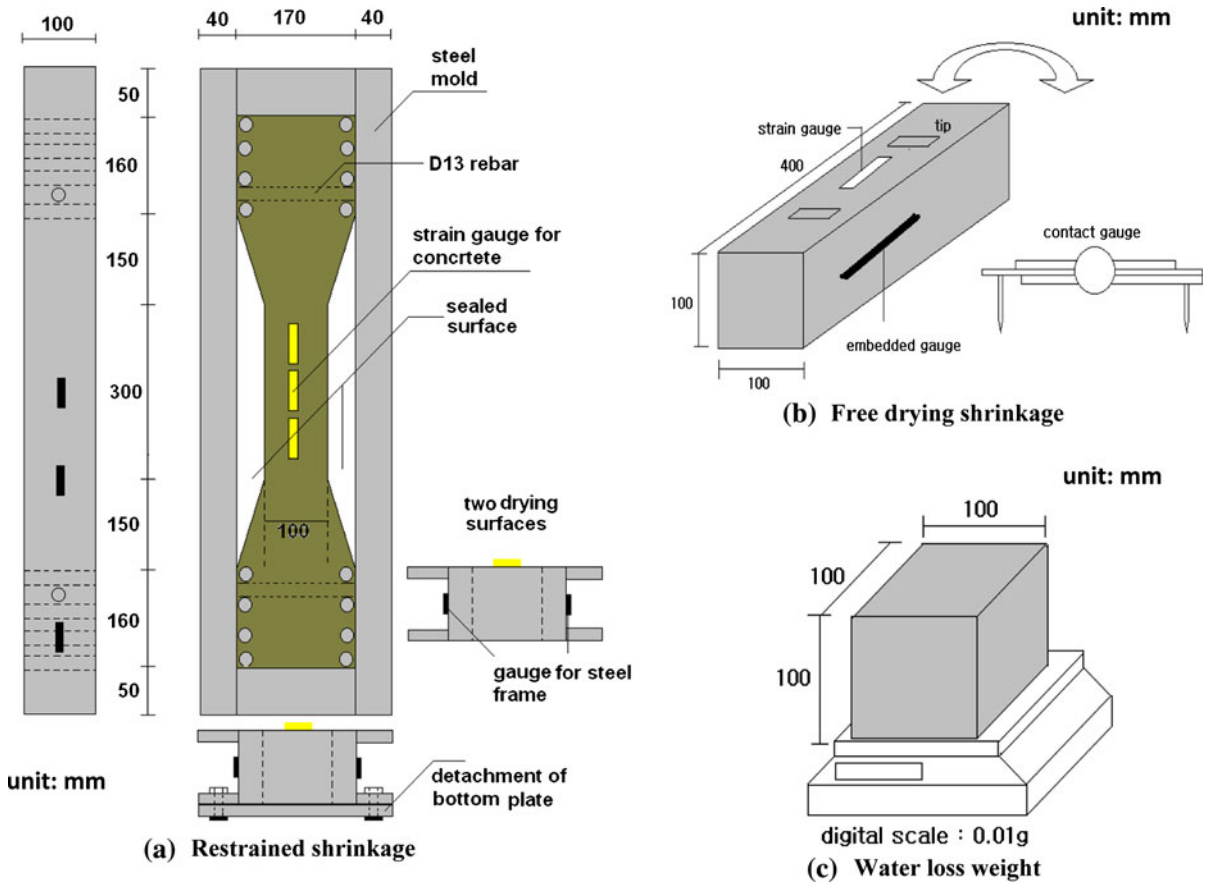

Fig. 1 Test equipments for shrinkage and water loss weight

Table 1 Mix proportion of concrete specimens

No	w/c	S/(S + G) (%)	Slump (cm)	G_{max} (mm)	Unit weight (kg/m^3)				Admixture (ml/m^3)		Chloride content	
					W	C	S	G	AE	water reducing	NaCl (kg/m^3)	% of cement wt
1	0.44	44.5	10	25	179.0	406.9	787.8	982.9	17.3	1951.0	0.0	0.00%
2											0.285	0.07%
3											2.436	0.60%
4											4.872	1.20%

W water, *C* cement, *S* Sand, *G* gravel, G_{max} maximum size of coarse aggregate, *AE* air entrainer

are obtained based on CEB/FIP model code [23], and they can be written as Eqs. 1 and 2, respectively:

$$f_c^{'}(t) = 23.7 \cdot \exp[0.2670 \times \{1 - (28/t)^{0.5}\}]^{0.5}, \quad t > 0 \tag{1}$$

$$E_c^{'}(t) = 20795.3 \cdot \exp[0.3127 \times \{1 - (28/t)^{0.5}\}]^{0.5}, \quad t > 0 \tag{2}$$

where, $f_c'(t)$, $E_c'(t)$, and t are compressive strength [MPa], elastic modulus [MPa], and time [day], respectively.

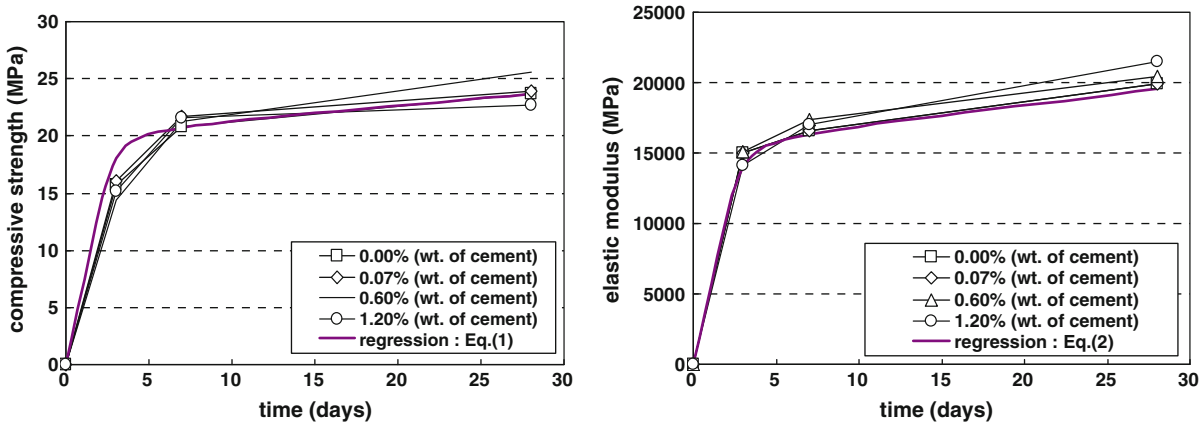

(a) Compressive strength (b) Elastic modulus

Fig. 2 Results for mechanical characteristics with NaCl content

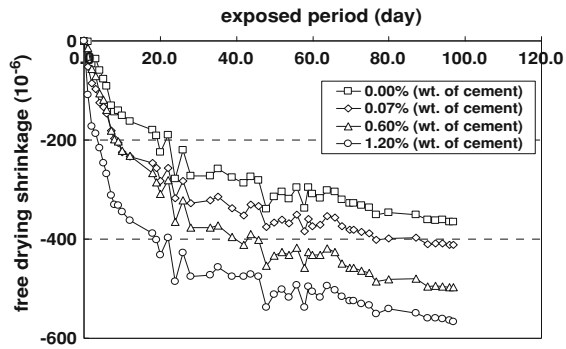

Fig. 3 Results for free shrinkage strain with NaCl content

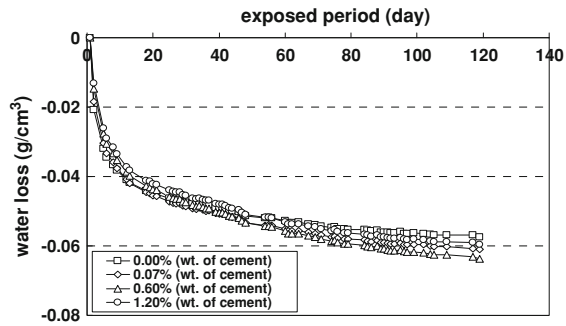

Fig. 4 Results for water loss weight with NaCl content

C_3S in NaCl solution is reported to show little effect on acceleration of hydration [24]. In this paper, NaCl is mixed in concrete so that no significant changes in mechanical properties are measured with different NaCl contents. Results showing little changes in hydration heat and strength in concrete with sodium chloride (NaCl) can be found also in previous research [1].

2.2.2 *Free drying shrinkage strain and water loss weight*

Free drying shrinkage in the specimens is measured and the results are shown in Fig. 3. The results in Fig. 3 are obtained from the average of the concrete gauges on the surface and embedded gauge. Those from dial gauge on tip are not utilized since they have big deviations. The results for water loss in the cubic specimen in control condition (R.H. 60% and temperature 20°C) are plotted in Fig. 4.

From the results in Figs. 3 and 4, it is evaluated that there is no clear relationship between mixed chloride contents and the amount of evaporated water. However, the free drying shrinkage increases significantly with increment of NaCl content. It can be assumed that changing density of pore water or chemically bound water due to chloride ions from NaCl is not the main reason for the increasing shrinkage in Fig. 3 since addition of chloride ions from NaCl in concrete does not cause more water evaporation as shown in Fig. 4. There are several parameters affecting drying shrinkage in concrete and chloride effect on drying shrinkage has been reported through experimental works. Shrinkage in concrete with sea water is reported to show higher shrinkage rate by 10–15% than normal concrete [25] and it increases up to 137% when chloride ion of 10,000 ppm is added to mix water in concrete [11]. When chloride ion is mixed in concrete, pore structure is changed to be more dense

morphology [26] and this changed pore structure may cause different behavior of drying shrinkage. In concrete with low alkalinity, drying shrinkage increases up to 20% in spite of similar water loss in concrete with high alkalinity [27]. Increased surface tension due to higher concentration of chloride ion [28] can cause higher drying shrinkage. However, it is also reported that concrete containing admixture causing pore refinement usually show higher drying shrinkage since drying shrinkage in concrete is directly associated with the water held by small pores in the size range 3 to 20 nm [29].

In this paper, changed pore radius with different chloride ions is assumed to be main activation of increasing shrinkage since the adopted model of drying shrinkage [2] is based on the capillary pore and tension, which is explained in Sect. 3.2.

3 Numerical analysis of shrinkage behavior with chloride ion

3.1 Concept of effective restrained strain

In order to evaluate cracking time due to restrained shrinkage, comparison with tensile strength and restraint stress which are dependent on time should be carried out. The tensile strength is assumed based on the results of compressive strength and it will be explained in Sect. 3.3. For derivation of effective restraint stress, effective restrained strain which is related to restrained shrinkage should be evaluated and converted to effective restraint stress. Effective restrained strain of the specimen which causes effective restraint stress can be defined as the difference between total restrained drying shrinkage strain and the free drying shrinkage strain. The each strain is experimentally measured for restraint and free condition as shown in Fig. 1a and b. In Fig. 5, total restrained strains from restraint condition are plotted with elapsed time, which are obtained from the average of three gauge measurements on the concrete surface.

In the Fig. 5, the initial point of measurement indicates the time of detachment of the bottom plate of the frame (2 days after casting) and the breaking point (x) indicates the cracking time, which means the release of the restraint stress from the mold. Volume changes caused by hydration expansion and

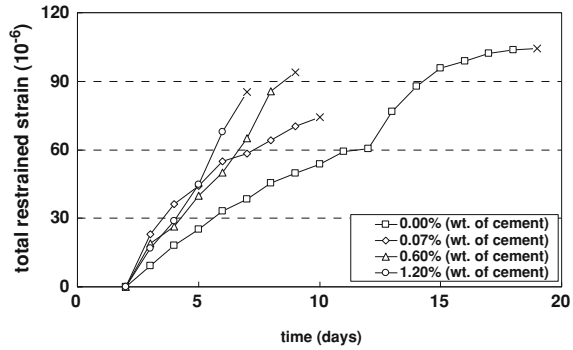

Fig. 5 Total restrained strain in restrained concrete with NaCl content

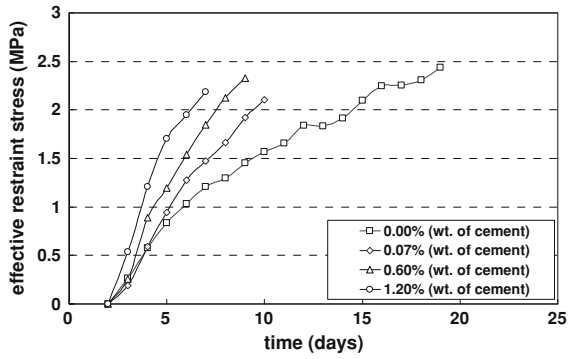

Fig. 6 Development of effective restraint stress with NaCl content

shrinkage actually occur before removing the bottom plate of the mold. However, it is very difficult to measure the strain in concrete before setting in the mold. For simplicity of restraint stress analysis, it is assumed that this period of 48 h before detachment of bottom plate is so short that its effect on drying shrinkage is not significant. The development of effective restraint stress in concrete is derived based on the effective restrained strain which is defined previously. It can be expressed as Eq. 3:

$$\sigma(t) = E_t(t) \cdot \varepsilon_{\mathrm{ef}}(t) = E_t(t) \cdot [\varepsilon_{\mathrm{restrained}}\ (t) - \varepsilon_{\mathrm{free}}\ (t)] \tag{3}$$

where $\varepsilon_{\mathrm{ef}}(t)$ is the effective restrained strain, $E_t(t)$ is the tensile elastic modulus of concrete which is assumed as the compressive elastic modulus in Eq. 2. $\varepsilon_{\mathrm{restrained}}\ (t)$ and $\varepsilon_{\mathrm{free}}\ (t)$ are the strains of total restrained drying shrinkage and free drying shrinkage, respectively. Figure 6 shows the results for effective restraint stress development through Eq. 3.

Concrete can be in crack-free condition so long as the tensile strength keeps higher than induced effective restraint stress. The results show rapid shortening of cracking time with the larger chloride content. It is shortened from 19.0 to 7.5 days with the increasing chloride content up to 1.20% of cement weight. The reason for the cracking is the increased effective restraint stress due to the chloride content. These experimental results will be compared with those from proposed analysis technique.

3.2 Modeling of shrinkage considering chloride effect

The relative humidity in the pore structure decreases with drying due to moisture gradient between exterior and interior concrete. Considering local thermodynamic and interface equilibrium, vapor and liquid interfaces would be formed in the pore structure due to the pressure differences caused by capillarity [30]. Where the interface is a part of an ideal spherical surface, this relation can be described by Kelvin's equation as in Eq. 4 [2, 30]:

$$\ln\left(\frac{P_v}{P_{v0}}\right) = -\frac{2\gamma M_w}{RT\rho_L}\frac{1}{r_s} \tag{4}$$

where, P_v/P_{v0} is relative humidity of vapor phase, γ is the surface tension of liquid water [N/m], M_w is molecular mass of water [kg/mol], R is universal gas constant [J/mol K], T is absolute temperature [K], ρ_L is density of liquid water [kg/m^3], r_s is a pore radius [m] in which the interface is created. Due to the surface tension of liquid water, the pressure of gas and liquid are not equal. This pressure difference (ΔP) would be described by Laplace's equation as Eq. 5. The idealized pore structure and interface equilibrium is shown in Fig. 7:

$$\Delta P = P_G - P_L = \frac{2\gamma}{r_s} \tag{5}$$

where, P_G and P_L are pressure of gas and liquid phase respectively [Pa].

The pressure of each phase can be computed by moisture transport model [15, 16]. From Eq. 5, it can be shown that the pressure of the liquid phase is lower than that of the gas phase, and tensile stress would act on pore walls where there is contact with the liquid phase. In this study, Shimomura's formulation [2] for capillary stress that causes drying shrinkage is adopted as Eq. 6:

$$\sigma_s = -\frac{2\cdot\gamma}{A_s r_s} = \frac{\rho_L\cdot R\cdot T}{A_s M_w\cdot\ln(P_v/P_{v0})} \tag{6}$$

where σ_s is tensile stress due to capillary tension [Pa], A_s area factor [m^3/m^3]. When elastic factor of capillary water (E_s) [Pa] is considered, the shrinkage strain (ε_{sh}) can be written as Eq. 7 [30]:

$$\varepsilon_{sh} = \sigma_s/E_s. \tag{7}$$

According to the previous research [15], E_s can be written as Eq. 8:

$$E_s = 1.333\times 10^4 f_c^{1/3} \tag{8}$$

where $f_c^{1/3}$ is compressive strength [kg/cm^2] from the previous model [31]. The magnitude of E_s as obtained from the above equation is reported to be about 25–50% of the ordinary value for the static elastic modulus of concrete [15]. The reason for this discrepancy might be the assumption of a uniform stress field due to capillary tension or perhaps some

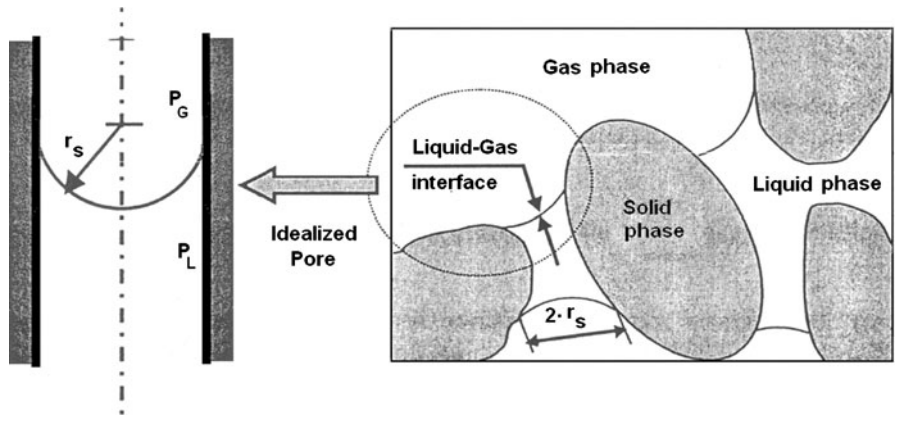

Fig. 7 Idealized structure of pores and interface equilibrium [15]

intrinsic differences in the mechanisms of deformation at micro- and macro scale due to capillary stress and that due to applied stress [15, 30]. When experimental results of compressive strength are considered in Eq. 8, the calculated E_s is approximately 40–50% of static elasticity in Fig. 2. In the constitutive relation of Eq. 7, linear elastic factor (E_s) is assumed to be 40% of static elastic modulus for the sake of simplicity of analysis. If the pore radius (r_s) decreases with chloride content, tensile stress of the pore liquid increases accordingly. In order to consider the reduced pore radius, exponential function for chloride content is assumed as Eq. 9. The shrinkage strain with chloride content can be written as Eq. 10 based on the linear relation:

$$r_s' = r_s \frac{1}{(1 + AC_{\mathrm{cl}}^B)} \tag{9}$$

$$\varepsilon_{\mathrm{sh}}' = \frac{\sigma_s}{E_s} \times (1 + AC_{\mathrm{cl}}^B) \tag{10}$$

where r_s' is pore radius in concrete with chloride content [m], $\varepsilon_{\mathrm{sh}}'$ is shrinkage strain considering chloride content (C_{cl}) [wt% of cement]. These equations are merged in analysis framework for calculation of cracking time. Utilizing the results shown in Fig. 3, increasing ratio of shrinkage due to chloride content can be evaluated. The results with different chloride content can be normalized by control data (results without chloride content) and an effect on shrinkage can be obtained with respect to chloride content. Among data in Fig. 3, those after 4 weeks showing relatively stable trend are selected and then normalized. The results are shown in Fig. 8. The constants of A and B in Eq. 9 are evaluated as 0.571 and 0.431 with correlation factor of 0.984.

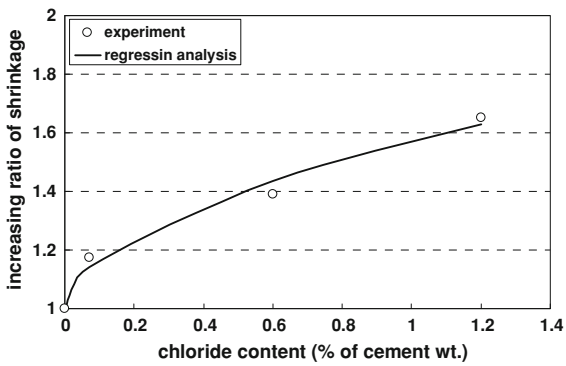

Fig. 8 Increasing ratio of shrinkage due to NaCl

3.3 Stress analysis of concrete under restraint shrinkage

The constitutive equations of bulk strain (ε_v) and deviatoric strain (e_{ij}) in axially restrained concrete can be written Eqs. 11 and 12 with mean stress (σ_v) and deviatoric stress (s_{ij}), respectively:

$$\varepsilon_v = \frac{1}{3K} \int (1 + \varphi) d\sigma_v + \varepsilon_t + \varepsilon_{\mathrm{sh}} - \varepsilon_{\mathrm{st}} \tag{11}$$

$$e_{ij} = \frac{1}{2G} \int (1 + \varphi) ds_{ij} \tag{12}$$

where K is bulk elastic modulus [Pa], G is shear modulus [Pa], φ is creep coefficient [−], ε_t is temperature strain [−], $\varepsilon_{\mathrm{sh}}$ is shrinkage strain [−], $\varepsilon_{\mathrm{st}}$ is the strain of restraining steel frame [−], respectively.

In this paper, previous model for creep function is used [23]. The shrinkage strain of the specimen ($\varepsilon_{\mathrm{sh}}$) in each time and spatial domain can be calculated by utilizing the previous models where chloride effect on shrinkage like Eqs. 9 and 10 is activated. The strain of the steel frame ($\varepsilon_{\mathrm{st}}$) is experimentally obtained from the gauge on the surface of the steel mold in Fig. 1. Therefore, the composition of various stresses caused by drying shrinkage due to the moisture transport and hydration, strain due to creep, and their integrated actions are considered in Eqs. 11 and 12. They can also be rewritten as Eq. 13 in the matrix form:

$$\{\sigma\} = [D]\{\varepsilon\} - \left\{ \int \varphi d\sigma \right\} - [D]\{\varepsilon_t + \varepsilon_{\mathrm{sh}} - \varepsilon_{\mathrm{st}}\} \tag{13}$$

where $[D]$is the stress–strain matrix.

Before cracking, Young's modulus calculated with hydration rate in each element represents that of concrete in the matrix $[D]$. The evaluation of cracking time in stress field is determined by the time when the tensile principal stress of each node is higher than the developed tensile strength due to hydration. The tensile strength of concrete (σ_t) is assumed as Eq. 14 based on experimental data of compressive strength utilizing CEB-FIP [23]:

$$\sigma_t = 0.0645 \cdot [237 \exp\{0.267 \times (1 - (28/t)^{0.5}\}^{0.5}]^{0.667}, \quad t > 0 \tag{14}$$

where σ_t is tensile strength of concrete [MPa]. The assumed tensile strength is 10.4–12.6% of compressive strength in Eq. 1.

3.4 Framework for evaluation of behavior in early-age concrete

In this section, previous models utilized for this study are briefly summarized and framework for evaluation of shrinkage behavior is introduced.

3.4.1 Multi-component hydration heat model (MCHHM) [15]

In view of concept of a multi-component powder material, the effect of different type of cement can be rationally taken into account to predict overall heat generation rate. The influence of variable moisture content of free water in the hydration is also taken into consideration in the concept. The chemical components of cement considered in this model are alite (C_3S), belite (C_2S), aluminate (C_3A), ferrite (C_4AF), and gypsum (CS_2H). Other powder materials like slag and fly ash can also be considered in the model as pseudo clinker components. The total heat generation rate of concrete (H) per unit volume is idealized as Eq. 15:

$$H = C \cdot H_c,\ H_c = \sum p_i H_i \tag{15}$$

where, C is powder content per unit volume of concrete, H_c is specific heat generation rate of cement, H_i is specific heat generation rate of individual clinker component and p_i is the corresponding mass ratio in cement to total mass. The temperature-dependant heat generation H_i of each clinker component is based on the modified Arrhenius's Law of chemical reaction, where various coefficients represent the interaction among the constituents as Eq. 16:

$$\bar{H}_i = \beta_i \gamma_i \mu_i \xi_i s_i \overline{H_{i,T_0}}(\overline{Q_i}) \exp\left\{-\frac{E_i(\overline{Q_i})}{R}\left(\frac{1}{T}-\frac{1}{T_0}\right)\right\},$$
$$\overline{Q_i} = \int \overline{H_i} dt \tag{16}$$

where, E_i is activation energy of ith component reaction, $\overline{H_{i,T_0}}$ is the referential heat generation rate when T_0 is 293 K, R is gas constant, β_i represents the reduction of probability of contact between unhydrated compound and free water. γ_i represents the retardation of cement and slag reaction caused by fly ash and organic admixture. μ_i represents the effect of mineral composition of Portland cement, ξ_i represents the reduction of the pozzolan's reaction due to the shortage of calcium hydroxide, s_i represents the effect of fitness of reaction particles. The heat rate of the entire cement (H_c) including blending powders, is given as the sum of the heat rate of all reaction as Eq. 17:

$$\begin{aligned}\overline{H_c} = \sum p_i \overline{H_i} =& p_{C_3S}\overline{H_{C_3S}} + p_{C_2S}\overline{H_{C_2S}} + p_{SG}\overline{H_{SG}} + \\ & p_{FA}\overline{H_{FA}} + p_{C_3A}(\overline{H_{C_3AET}} + \overline{H_{C_3A}}) \\ & + p_{C_4AF}(\overline{H_{C_4AFET}} + \overline{H_{C_4AF}}).\end{aligned} \tag{17}$$

3.4.2 Mirco-pore structure formation model (MPSFM) [15]

For analytical purpose, the interlayer porosity is simply lumped with the porosity distributions of gel and capillary porosity to obtain the total porosity distribution of cement paste as Eq. 18:

$$\begin{aligned}\varphi(r) &= \varphi_{lr} + \varphi_{cg}(r) \\ &= \varphi_{lr} + \frac{1}{\varphi_{cp}+\varphi_{gl}}[\varphi_{cp}(r) + \varphi_{gl}(r)]\end{aligned} \tag{18}$$

where, r is the pore radius, φ_{lr} is the interlayer porosity, and φ_{cg} is the combined porosity distribution of capillary porosity (φ_{cp}) and gel porosity (φ_{gl}). Each of the capillary and gel porosity distribution ($\varphi_{cp}(r)$ and $\varphi_{gl}(r)$) are represented by a simplistic Rayleigh–Ritz (R–R) distribution function as Eq. 19:

$$\begin{aligned}&V_i = 1 - \exp(-B_i r),\ (0 \le V(r) \le 1), \\ &dV_i = B_i r \exp(-B_i r) d\ln(r)\end{aligned} \tag{19}$$

where, V_i expresses a fractional pore volume of the distribution up to pore radius (r) and B_i is the sole porosity distribution parameter. A bimodal analytical porosity (φ_{total}) distribution of the cement paste can be obtained as Eq. 20:

$$\begin{aligned}\varphi_{total} = \varphi_{lr} &+ \varphi_{gl}[1 - \exp(-B_{gl} r)] \\ &+ \varphi_{cp}[1 - \exp(-B_{cp} r)]\end{aligned} \tag{20}$$

where, B_{cp} and B_{gl} are distribution parameters correspond to capillary and gel porosity components. If the porosity is a cylindrical shape in such a distribution, then the pore distribution parameter (B_i) can be obtained form the following relationship of Eq. 21:

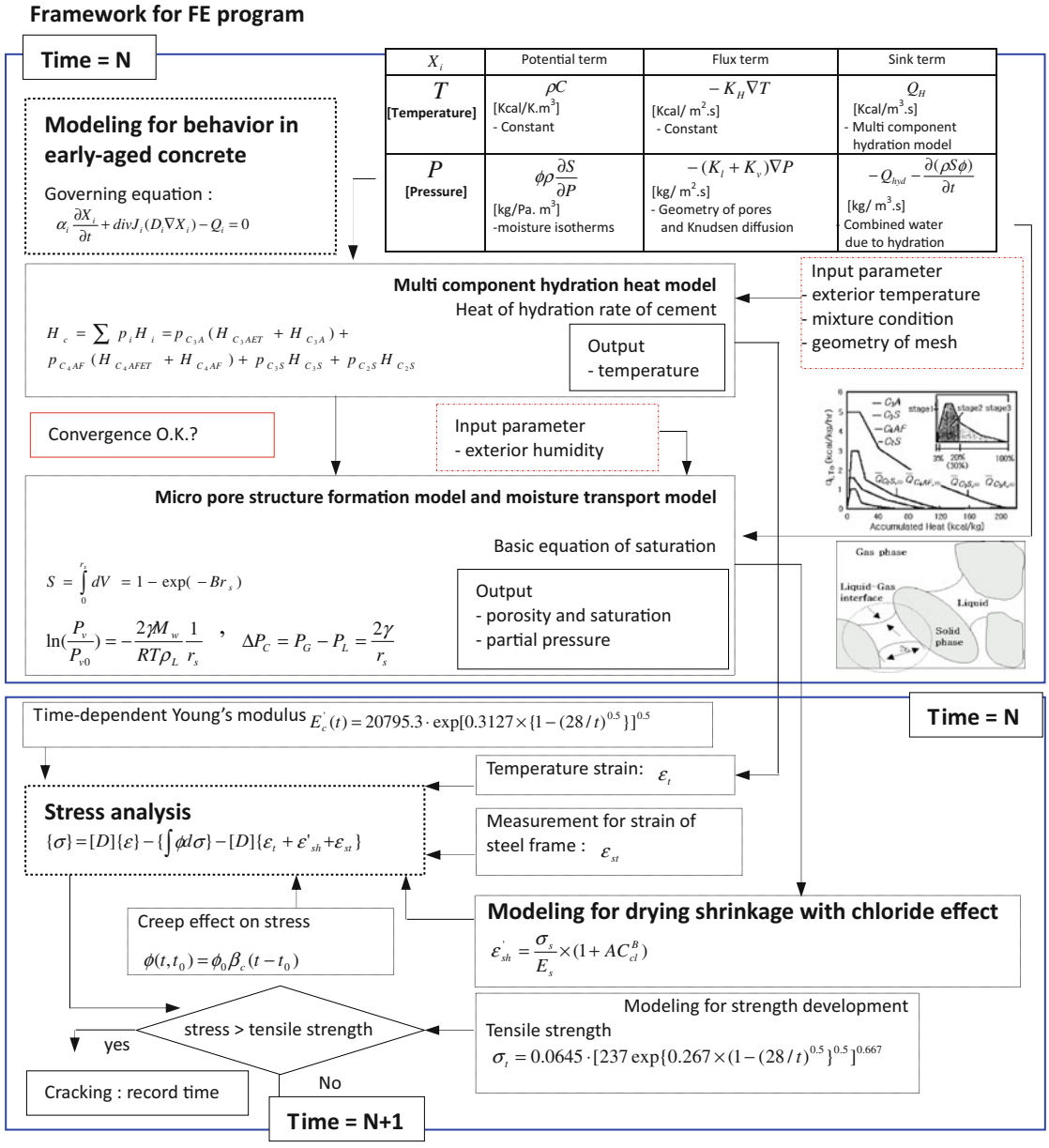

Modeling parameters [15]

ρC : specific heat capacity, K_H : heat conductivity, Q_H : heat generation rate, K_l : liquid conductivity, K_v : vapor conductivities, Q_{hyd} : combined water due to hydration, H_c : specific heat generation rate of blended cement, p_i : corresponding mass ratio, H_i : dependent heat generation rate in clinker component (i), S : saturation, B : pore structure parameter, ϕ_0 : function of relative humidity, strength, and shape of specimen, β_c : function of time and shape, t_0 : loading time

Fig. 9 Schematic view of FE analysis in this study

$$S_{\text{sur}} = 2\varphi_i \int r^{-1} dV = 2\varphi_i \int_{r_{\min}}^{\infty} B\exp(-Br) d\ln(r) \tag{21}$$

where S_{sur} is surface area per unit volume of the matrix, $r_{\min}$ is the minimum pore radius. This expression cannot be solved analytically as a closed-form solution so that an explicit relationship is adopted, which has been obtained by fitting the accurate numerical evaluations of the above integral for a large number of data-sets which relate B as a function of S_{sur}/φ [15, 16]. If the porosity distribution of the microstructure is known, Eq. 22 which is derived from Kelvin's equation enables to obtain the amount of water present in the microstructure at a given ambient relative humidity. By integrating the pore volume that lies below pore radius (r_s), saturation (S) can be written as Eq. 23 through a porosity distribution V given by Eq. 19:

$$r_s = -\frac{2\gamma M_w}{\rho_L RT \ln(h)}, \tag{22}$$

$$S = \int_0^{r_s} dV = 1 - \exp(-B_i r_s) \,(\text{for wetting condition}), \tag{23}$$

where, h is relative humidity of vapor phase. The expression for saturation (S) is changed with hysteretic behavior of isotherm.

Each model is well explained and documented in following references [15–19].

3.4.3 *Framework for this study*

In order to evaluate cracking time caused by effective restraint stress, framework for FE analysis is required with covering the behavior of early-age concrete like hydration, micro pore structure, and moisture transport. In this paper, integrated analysis program DuCOM [15, 16] is utilized for the evaluation of the behaviors in early-age concrete and stress analysis. Schematic view of unified FE analysis is shown in Fig. 9 including the chloride effect on pore radius and shrinkage.

4 Comparison and verification

In the integrated FE analysis, the thermal deformation and drying shrinkage strain in early-age concrete, and equivalent stress in each restrained condition are calculated through previous models (MCHHM, MPSFM, and MTM) considering chloride effect on shrinkage strain. Each Gaussian point in element has different strength with different hydration rate due to exterior condition, and the changed strength with time and space is considered for evaluation of crack resistance. The boundary and initial conditions for the analysis are shown in Table 2 with FE mesh for specimen.

The results for free drying shrinkage strain of specimen with chloride content are shown in Fig. 10. The comparison with restraint stress and tensile strength is shown in Fig. 11 with different NaCl contents. In Fig. 12, cracking time and effective restraint stress from experiment are compared with those from the proposed analysis technique. Effective restraint stress at the age of 7 days are shown since no cracking in all the cases (0.0–1.2% of chloride content) occurs in this period.

In Fig. 12, there is slight difference of stress between numerical and experimental data in initial condition, however, those from the proposed technique seem to be reasonably modeled through reverse analysis for the increased effective restraint stress and shortened cracking time caused by chloride content.

Table 2 Conditions and mesh for FE analysis

Period	Temperature	Relative humidity
0–2 days (curing)	25°C	R.H 100%
After 2 days (drying period)	20°C	R.H. 60%

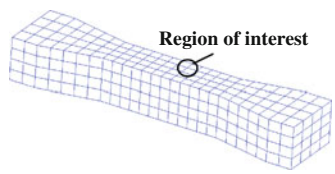

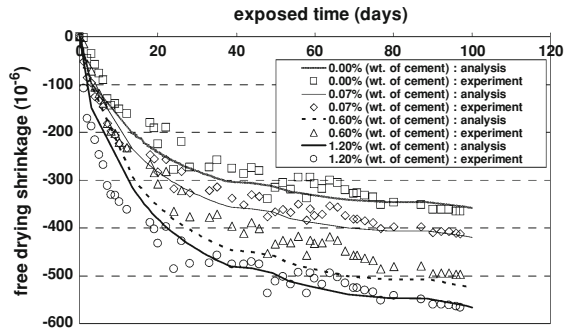

Fig. 10 Comparison of free shrinkage with NaCl content

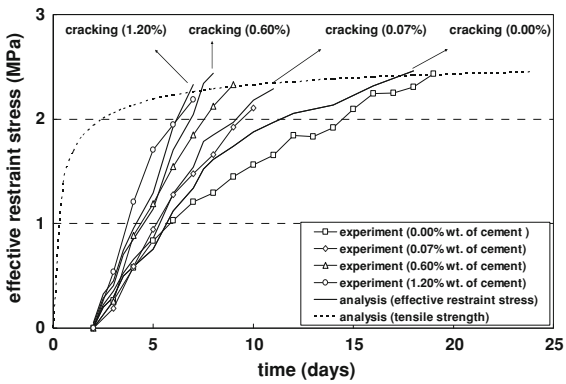

Fig. 11 Comparison of effective restraint shrinkage stress with NaCl content

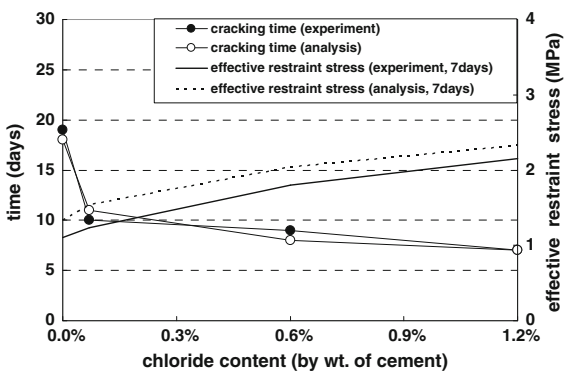

Fig. 12 Comparison of cracking time and effective restraint stress

The proposed technique shows reasonable prediction of shrinkage behavior in chloride contaminated concrete but still has several limitations and considerations to be modified. There are several parameters on drying shrinkage in chloride-mixed concrete like changes in pore structure, a degree of alkali, and surface tension. Among these parameters, only change in pore radius is assumed and considered in the model. Surface tension should increase when chloride ions exist in pore water but same surface tension (72 mN/m) is used. E_s for drying shrinkage strain is assumed as 40% of static elastic modulus based on the previous research and experimental results. This factor (E_s) can be modified in the quantitative manner. For this study, several previous models of MCHHM, MPSFM, and WTM are utilized. In the MCHHM, The chemical components of cement are considered. The heat generation of each clinker compound is based on a modification of the Arrhenius law of chemical reaction. In the MPSFM, total porosity can be obtained through bimodal analytical distribution function. Unfortunately, the effect of chemical admixture like air entrainer is not considered in the MPSFM. If the modeling for the performance of chemical admixture is included, the proposed technique can predict the drying shrinkage behavior more reasonably and quantitatively.

5 Conclusions

The conclusions on analysis technique for restrained shrinkage of concrete containing chlorides are as follows.

(1) By the tests for compressive strength, Young's modulus, water loss, and drying shrinkage for early-age concrete with different chloride contents, it is evaluated that the increased chlorides from NaCl in concrete has little effect on the strength, Young's modulus, and water loss of concrete. However, it causes significantly increased drying shrinkage strain and makes cracking time shortened by increasing restraint stress.

(2) The integrated analysis technique considering the chloride effect on drying shrinkage is proposed by utilizing the previous models for behavior in early-age concrete based on the thermodynamics equilibrium relation. Through reverse analysis, the proposed technique is able to model the increasing restraint stress and the reduced cracking time due to higher chloride contents under confined condition.

Acknowledgment The coauthor of this paper, Prof. Ha-Won, Song has passed away and I would like to honor him for his

contributions to this study and the researches on concrete. The authors also appreciate Prof. Koichi Maekawa of the University of Tokyo for the valuable advices. The author, Seung-Jun, Kwon appreciates a grant (06-CIT-A02: Standardization Research for Construction Materials) from Research Policy/Infrastructure Development Program funded by Ministry of Land, Transport and Maritime Affairs of Korea government.

References

1. Song HW, Cho HJ, Park SS, Byun KJ, Maekawa K (2001) Early-age cracking resistance evaluation of concrete structure. Concr Sci Eng 3:62–72
2. Shimomura T, Maekawa K (1997) Analysis of the drying shrinkage behavior of concrete using a micromechanical model based on the micro pore structure of concrete. Mag Concr Res 49:303–322
3. Chaube RP, Shimomura T, Maekawa K (1993) Multiphase water movement in concrete as a multi-component system. In: Proceedings of the 5th RILEM international symposium on creep and shrinkage, Barcelona. E&FN Spon, London
4. Song HW, Park SS, Byun KJ (2001) Analysis of chloride penetration in cracked concrete at early age. J KSCE 21:915–924 (in Korean)
5. Song HW, Pack SW, Lee CH, Kwon SJ (2006) Service life prediction of concrete structures under marine environment considering coupled deterioration. J Restor Build Monum 12:265–284
6. Song HW, Kwon SJ, Byun KJ, Park CK (2006) Predicting carbonation in early-aged cracked concrete. Cem Concr Res 36:979–989
7. Aoki Y, Shimomura T, Obata H (1999) Stress analysis and cracking criteria of concrete under restrained drying shrinkage. In: The 7th East Asia-Pacific conference on structural engineering and construction, pp 1425–1430
8. Ishida T, Maekawa K (2003) Modeling of durability performance of cementitious materials and structures based on thermo-hygro physics. In: RILEM Proceedings PRO 29, Life prediction and aging management of concrete structures, pp 39–49
9. Cho HJ, Song H-W, Byun KJ (2003) Development of analytical model on setting characteristics of early-age concrete. J KSCE 23:549–557 (in Korean)
10. Kdroff J, Hilsdorf HK (1995) Performance criteria for concrete durability, RILEM Report 12, Rilem. E & FN SPON, London
11. KICTTEP (2000) Development of quality and durability improvement of concrete using sea sand-Part2, Quality control and evaluation of durability in concrete with sea sand. Technical Report R&D/97-0001 (in Korean)
12. Andrade C (1993) Calculation of chloride diffusion coefficients in concrete from ionic, migration measurements. Cem Concr Res 23:724–742
13. Gérard B, Marchand J (2000) Influence of cracking on the diffusion properties of cement-based materials part 1: influence of continuous cracks on the steady-state regime. Cem Concr Res 30:37–43
14. Broomfield JP (1997) Corrosion of steel in concrete: understanding, investigation and repair. E&FN SPON, London
15. Maekawa K, Chaube RP, Kishi T (1999) Modeling of concrete performance: hydration, microstructure formation and mass transport. Routledge, London and New York
16. Ishida T, Chaube RP, Maekawa K (1996) Modeling of pore content in concrete under generic drying wetting conditions. Concr Libr JSCE 18:113–118
17. Mabrouk R, Ishida T, Maekawa K (2004) A unified solidification model of hardening concrete composite for predicting the young age behavior of concrete. Cem Concr Compos 26:453–461
18. Ishida T, Maekawa K, Kishi T (2007) Enhanced modeling of moisture equilibrium and transport in cementitious materials under arbitrary temperature and relative humidity history. Cem Concr Res 37:565–578
19. Nakarai K, Ishida T, Kishi T, Maekawa K (2007) Enhanced thermodynamic analysis coupled with temperature-dependent microstructures of cement hydrates. Cem Concr Res 37:139–150
20. Japan Standard Association (2002) Method of test for drying shrinkage cracking of restricted concrete, JIS A 1151 (in Japanese)
21. Japan Standard Association (2001) Method of test for static modulus of elasticity of concrete, JIS A 1149 (in Japanese)
22. Japan Standard Association (2002) Method of test for compressive strength of concrete, JIS A 1108 (in Japanese)
23. CEB/FIP (1990) Model Code Comité Euro-International du béton
24. Brown PW, Harner CL, Prosen EJ (1986) The effect of inorganic salts on tricalcium silicate hydration. Cem Concr Res 16:17–23
25. Park DK, Yang KY (2006) A study on modeling of prediction of drying shrinkage according to properties of aggregate. Korean Ins Build Const 6:73–77
26. Suryavanshi AK, Scantlebury JD, Lyon SB (1995) Pore size distribution of OPC & SRPC mortars in presence of chlorides. Cem Concr Res 25:980–988
27. Smaoui N, Be′rube′ MA, Fournier B, Bissonnette B, Durand B (2005) Effects of alkali addition on the mechanical properties and durability of concrete. Cem Concr Res 23:203–212
28. Vanhanen J, Hyvarinen1 A-P, Anttila1 T, Raatikainen T, Viisanen Y, Lihavainen H (2008) Ternary solution of sodium chloride, succinic acid and water; surface tension and its influence on cloud droplet activation. Atmos Chem Phys 8:4595–4604
29. Mehta PK, Monteiro PJM (2006) Concrete: microstructure properties and materials, 3rd edn. McGraw-Hill, New York
30. Ishida T, Chaube RP, Kishi, T, Maekawa K (1997) Microphysical approach to coupled autogeneous and drying shrinkage of concrete. In: Proceedings of JSCE 578/V-37
31. Kato Y, Kishi T (1994) Strength development model for concrete in early ages based on hydration of constituent minerals. Proc JCI 16(1):503–508